Relaxation properties in a diffusive model of *k*-mers with constrained movements on a triangular lattice

J. R. Šćepanović,[1] I. Lončarević,[2] Lj. Budinski-Petković,[2] Z. M. Jakšić,[1] and S. B. Vrhovac[1,*]

[1]*Institute of Physics, University of Belgrade, Pregrevica 118, Zemun 11080, Belgrade, Serbia*
[2]*Faculty of Engineering, Trg D. Obradovića 6, Novi Sad 21000, Serbia*

We study the relaxation process in a two-dimensional lattice gas model, based on the concept of geometrical frustration. In this model the particles are *k*-mers that can both randomly translate and rotate on the planar triangular lattice. In the absence of rotation, the diffusion of hard-core particles in crossed single-file systems is investigated. We monitor, for different densities, several quantities: mean-square displacement, the self-part of the van Hove correlation function, and the self-intermediate scattering function. We observe a considerable slowing of diffusion on a long-time scale when suppressing the rotational motion of *k*-mers; our system is subdiffusive at intermediate times between the initial transient and the long-time diffusive regime. We show that the self-part of the van Hove correlation function exhibits, as a function of particle displacement, a stretched exponential decay at intermediate times. The self-intermediate scattering function (SISF), displaying slower than exponential relaxation, suggests the existence of heterogeneous dynamics. For each value of density, the SISF is well described by the Kohlrausch-Williams-Watts law; the characteristic timescale $\tau(q_n)$ is found to decrease with the wave vector q_n according to a simple power law. Furthermore, the slowing of the dynamics with density ρ_0 is consistent with the scaling law $1/\tau(q_n; \rho_0) \propto (\rho_c - \rho_0)^\varkappa$, with the same exponent $\varkappa = 3.34 \pm 0.12$ for all wave vectors q_n. The density ρ_c is approximately equal to the closest packing limit, $\theta_{\mathrm{CPL}} \lesssim 1$, for dimers on the two-dimensional triangular lattice. The self-diffusion coefficient D_s scales with the same power-law exponent and critical density.

PACS number(s): 05.40.−a, 61.20.Ja, 61.20.Lc, 64.70.P−

I. INTRODUCTION

In recent years, systems exhibiting anomalous subdiffusive behavior have attracted growing attention in various fields of physics and related sciences. The signature of subdiffusion is that the mean-square displacement of the diffusing species grows sublinearly with time. There are many examples of physical systems that exhibit such anomalous transport; they involve complex systems, disordered systems, semiconductors, polymers, glasses, turbulent plasma, and many others [1]. Subdiffusion has been detected experimentally in several systems, such as porous materials [2], glass-forming systems [3,4], and biological media [5,6].

The prediction of transport properties from microstructure of porous media remains a focus of research in physics and engineering. Commonly, microporous materials contain pores of the size of the diffusing molecules. Tight confinement of molecules results in a very different behavior of molecules as compared to free gas. Zschiegner *et al.* [7] used the model pores with fractal structure to study the diffusion of particles colliding with the pore walls. One of the interesting results was the presence of anomalous diffusion in the linear two-dimensional (2D) channels if angular reflection is inhomogeneous. Very recently, anomalous transport has been found in the molecular dynamics simulations for mixtures of mobile and immobile spherical particles [8–10]. This picture can be understood as a cartoon of the dynamics of fluids confined in disordered porous matrices. Finally, a theoretical study has recently been carried out for the slow dynamics of a tagged particle moving in a fluid absorbed in a disordered porous

solid within the framework of the mode-coupling theory [11]. Using simple models with pure hard-core interactions, it was shown that the diffusion-localization transition is characterized by the emergence of various dynamical anomalies, and in particular, by the appearance of a subdiffusive behavior of the mean-square displacement.

Diffusion of particles, which occurs in channels so narrow that the particles are unable to pass each other, is usually referred to as single-file diffusion (SFD) [12]. This physical situation is encountered in many systems, such as ion transport in biological membranes [13], and molecules channeling in zeolites [12]. The absence of particle exchange leads to the well-known prediction that the mean-square displacements in infinite, single-file systems increase with the square root of time [14]. As soon as the nanochannels interpenetrate each other, they give rise to the formation of channel networks. In mutually intersecting channel arrays, molecular diffusion in different directions may be correlated between each other. Important examples of materials, which might exhibit such a behavior, are zeolites of MFI structure type like ZSM-5 [15]. Mutually intersecting arrays of single-file systems can serve as a model system for the zeolite catalysis by directing the reactant and product molecules along different intracrystalline channels [16].

In this paper we introduce a 2D lattice gas model that has both translational and rotational degrees of freedom. Our model is based on the diffusional dynamics of *k*-mers on a planar triangular lattice, similar to the diffusive model of dimers on a square lattice proposed by Fusco *et al.* [17,18]. In the following, we sketch the main features of our model, along the lines of Ref. [19]. The system is initialized by the random sequential adsorption (RSA) model [20]. In

*vrhovac@ipb.ac.rs; http://www.ipb.ac.rs/vrhovac/

two dimensions, RSA is a typical model for irreversible and sequential deposition of macromolecules at solid-liquid interfaces [21,22]. The kinetic properties of a deposition process are described by the time evolution of the coverage $\rho(t)$, which is the fraction of the substrate area covered by the adsorbed particles. In this process k-mers are adsorbed, one at a time, at randomly chosen sites of a triangular lattice, subject to constraints imposed by interaction with previously deposited k-mers. At a chosen value of the coverage, the deposition is turned off and diffusion of k-mers is initiated. The only interactions between the particles are the geometrical ones, i.e., we allow only the single-k-mer moves that do not cause double occupation at any site at any time. At each Monte Carlo step, the moves of a randomly chosen k-mer can be either translation along its axis or rotation when the k-mer changes its orientation. In the absence of rotation, a k-mer can move only along one of the three crystal axes. In this case, we investigate the diffusion of hard core particles in crossed single-file systems. Our model is designed as a model for cooperative dynamics rather than for a concrete physical system. A characteristic feature of such cooperativity is that the movements of individual particles are correlated, even at long time periods, because the displacement of a given particle over a long distance necessitates the motion of many other particles in the same direction. Our main goal is to show that there are occasions where a simple geometrical restriction to diffusion and flow can give rise to "anomalous" behavior.

One of the aims of this paper is to employ a densely packed lattice model for capturing the physical mechanism underlying the non-Gaussianity of glassy dynamics [23]. First, we focus on the non-Fickian character of single particle displacements. We show that the mean-squared displacements exhibit a subdiffusive behavior at intermediate times between the initial transient and the long-time diffusive regime. To detect the presence of dynamical heterogeneities, we investigate the time dependence of the self-part of the van Hove correlation function, which represents the probability distribution of the particle displacements. Generally a system is considered as dynamically heterogeneous if dynamically distinguishable populations of particles with different mobilities (e.g., "fast" or "slow" particles) can be isolated by a computer simulation or experiment. We show that the van Hove correlation function [Eq. (3)] at intermediate times deviates from a Gaussian distribution expected for a Fickian diffusion. Its deviations from the Gaussian behavior are usually ascribed to the presence of particles that are substantially faster or slower than the average [24,25]. The focal point of our discussion is the intermediate scattering function, which is a measure of the time decorrelation of the positional wave vectors. We evaluate the relaxation times by studying the time decay of the self-part of the intermediate scattering function [Eq. (6)]. In particular, we analyze the relaxation time dependence both on the wave vector (length scale) and on the density of the system. Most of our attention is focused on the diffusion of dimers, although we present some results for other k-mers ($k > 2$) for comparison. We concentrate here on the influence of the length of the k-mers on the temporal behavior of MSD and SISF.

In Sec. II we introduce our model and give some details of our simulations. We present the simulation results and

discussions in Sec. III. Finally, Sec. IV contains additional comments and final remarks.

II. MODEL AND DETAILS OF THE SIMULATIONS

The stochastic process that we investigate in this paper consists of the random diffusion of k-mers on a triangular lattice with fixed density. The adsorbing objects are k-mers covering $k = 2$, 3, and 4 sites. The initial state of the system is prepared through the RSA of k-mers in two dimensions. For this purpose we perform the Monte Carlo procedure of filling the triangular lattice by inserting the k-mers randomly up to the chosen coverage fraction ρ_0. We start with an initially empty triangular lattice. At each Monte Carlo step a lattice site is selected at random. If the selected site is unoccupied, one of the six possible orientations is chosen at random, and deposition of the object is tried in that direction. We fix both the direction and the beginning of the k-mer at the selected site and search whether k consecutive sites in chosen direction are unoccupied. If so, we occupy these k sites and place the k-mer. If the attempt fails, a new site is selected, and so on. Once a k-mer is placed it affects the geometry of all later placements, so the dominant effect in RSA is the blocking of the available lattice area. After long enough time a jamming limit $\rho_{\text{jam}}^{(k)}$ is reached when there is no more possibility for a deposition event. However, the deposition process is stopped when the coverage fraction reaches the chosen value $\rho_0 < \rho_{\text{jam}}^{(k)}$. In this way we are able to prepare the system in disordered initial state with a statistically reproducible density ρ_0.

Then, for each initially prepared configuration, we switch the deposition events off and initiate a random diffusive dynamics in our model. In this way we are able to follow the dynamics of the system in an equilibrium regime. At this stage, apart from the hard core interaction there are no other interactions between the particles. We allow only the single-k-mer moves that do not cause a double occupation at any site at any time. There are two kinds of moves that we could allow: moves in which a k-mer simply translates along its axis, which we call a glide, or moves in which a k-mer changes its orientation, which we call a rotation.

In our algorithm, a diffusion event is tried only if there is a beginning of a deposited k-mer at the randomly selected site, otherwise the attempt is rejected. Then we pick one of the two possible directions along the k-mer axis at random, with equal probability, and try to move the selected k-mer by one lattice spacing in that direction. The k-mer is moved if it does not overlap with any of the deposited k-mers. If the attempted move is not possible, the k-mer stays at its original position. Therefore, if only glide moves are allowed in the model, k-mers oriented along any of the three axis bisecting the triangular lattice are considered separately, and their orientations are kept fixed without allowing rotations. The subdiffusion appears naturally as a consequence of these constrained movements and is not an additional ingredient of the model. We shall return to this point later in connection with the interplay between the kinetic constraints and diffusional dynamics.

If both rotations and glides of k-mers are allowed, a single k-mer can move in any of the six possible directions, so that particle simply performs a random walk on the triangular

lattice. In our model the glide and rotation attempts are statistically independent, and they perform sequentially with corresponding probabilities. At each Monte Carlo step a glide is attempted with probability $P_{gl} = 1$ and rotation with probability P_{rot}. Algorithm for a glide move of a randomly chosen k-mer was already described in details in the paragraph above. Each glide attempt is followed by a rotation attempt with probability P_{rot}. The rotation process starts by choosing a lattice site at random. If this selected site is unoccupied, the rotation step fails and the process continues by choosing a new site for the glide attempt. On the other hand, if a beginning of a deposited k-mer is at the selected site, one of the six possible orientations is chosen at random, and rotation of the k-mer is tried with probability P_{rot} in that direction. The object is rotated if it does not overlap with any of the deposited objects. On the contrary, the attempt is rejected.

The Monte Carlo simulations are performed on the triangular lattice of size $L \times L = 60^2$ with a periodic boundary condition. For convenience we have assumed that the lattice spacing is one. The time is counted by the number of glide attempts and scaled by the total number of lattice sites. We covered densities ρ_0 between 0.10 and $\rho_{jam}^{(2)} = 0.9139 \pm 0.0004$ [26,27], which corresponds to 180 dimers at the lowest density $\rho_0 = 0.10$ and 1638 dimers at the highest density, $\rho_0 = 0.91$. The data are averaged over 20 independent runs for each of the investigated densities.

III. RESULTS

In this section we present and discuss the results of our simulations. The first subsection deals with the mean-square displacement of the particles, and the next subsections with the density-density autocorrelation functions.

A. Mean-square displacement

Dynamical behavior of our lattice model at large length scales is studied via the mean-square displacement (MSD) of a particle, $\langle \Delta r^2(t) \rangle$. It is defined as

$$\langle \Delta r^2(t) \rangle = \frac{1}{N} \left\langle \sum_{i=1}^{N} |\vec{r}_i(t) - \vec{r}_i(0)|^2 \right\rangle, \quad (1)$$

where $\vec{r}_i(t)$ is the position of the ith particle at time t, and N is the number of k-mers, i.e., $N = \rho_0 L^2/k$. The angular brackets $\langle \cdot \rangle$ here and in the following denote an average over the simulation ensemble in which the coverage fraction ρ_0 of the system is fixed. Anomalous diffusion is characterized by the occurrence of a MSD of the form

$$\langle \Delta r^2(t) \rangle = K_\alpha t^\alpha, \quad (2)$$

where the exponent α classifies the different types of diffusion: subdiffusion for $0 < \alpha < 1$, normal diffusion for $\alpha = 1$, and superdiffusion for $1 < \alpha \leqslant 2$; for $\alpha = 2$ the process is called ballistic [1,28]. In the following, we shall deal with the subdiffusive domain $0 < \alpha < 1$.

We first consider the dynamical properties of dimers ($k = 2$) when only glide moves are allowed (i.e., $P_{rot} = 0$). In this case, our model can serve as an example of mutually intersecting arrays of single-file systems. In Fig. 1 we plot the MSD as
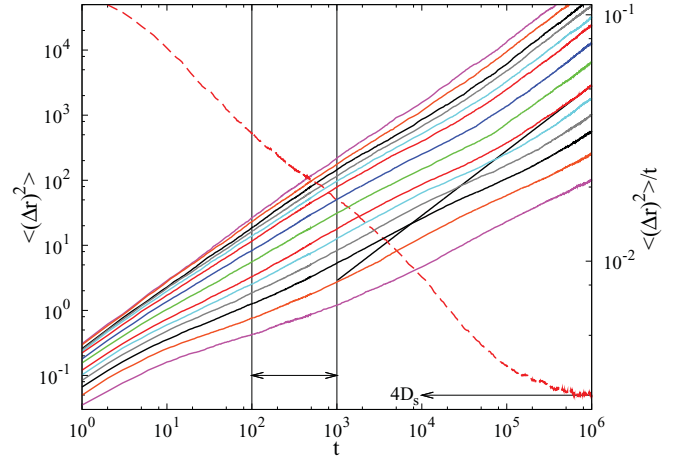

FIG. 1. (Color online) Double logarithmic plot of the temporal evolution of the MSD for dimers at various densities ρ_0. The solid lines represent the MSD vs time t for densities $\rho_0 = 0.10, 0.15, 0.20, 0.25, 0.30, 0.35, 0.45, 0.55, 0.65, 0.70, 0.75, 0.80, 0.85, 0.90$, from top to bottom (left-hand axis). The dashed line is plotted against the right-hand axis and gives the temporal evolution of the MSD divided by t, for density $\rho_0 = 0.65$. The horizontal arrow at $4D_s = 2.9 \times 10^{-3}$ represents the average value of $\langle \Delta r^2(t) \rangle/t$, for large t. Additionally, the slanted straight line is shown, indicating the late-time diffusive behavior, $\langle \Delta r^2(t) \rangle = 4D_s t$, in the case of $\rho_0 = 0.65$. The values of exponent α [Eq. (2)] reported in Table I are obtained from the slopes of the MSD vs t curves in the time region between the thin vertical lines.

a function of time for several different densities, in the range $\rho_0 = 0.10$–0.90. Also included in Fig. 1 (dashed line) is the temporal evolution of the MSD divided by t, $\langle \Delta r^2(t) \rangle/t$, for density $\rho_0 = 0.65$. In that case, normal diffusion yields a line of slope 0, and subdiffusion yields a line of negative slope. Additionally, a thin straight line with the unit slope is shown, indicating the late-time diffusive behavior and the linear fit to dimer displacement, $\langle \Delta r^2(t) \rangle \propto t$. For high densities our results indicate that three distinct regimes of the MSD can be distinguished. At short times dimers do not feel the presence of the neighbors, and they move freely. After a few time steps corresponding to the initial transient, we observe that the system is subdiffusive. Region of anomalous diffusion extends over several decades of time, before eventually entering the diffusing regime. As seen from Fig. 1, the region of anomalous diffusion increases with ρ_0. For densities $\rho_0 \gtrsim 0.75$ a sublinear time dependence extends until the limit of our simulations ($t = 10^6$). However, for lower densities we observe that the MSD reaches a linear time behavior (diffusive regime) within the length of the simulation. For certain time regions, it is possible to fit the MSD data with a power law (2). Values of the fitting parameter α are determined from the slopes of $\langle \Delta r^2(t) \rangle$ versus t curves in the range $t \in [10^2, 10^3]$ (see Fig. 1). The corresponding values of parameter α, obtained for different densities ρ_0, are reported in Table I with an uncertainty of calculation $\delta\alpha \leqslant 0.005$. The exponent α is less than one for all the coverages considered and decreases with the density ρ_0. As expected, in the limiting case of very low densities, the value of exponent α tends to one; the subdiffusion at intermediate

TABLE I. Values of the parameter α [Eq. (2)] for dimers obtained from the fit to the power law (2) of the MSD in the range $t \in [10^2, 10^3]$ for various densities ρ_0.

ρ_0	α
0.100	0.956
0.150	0.921
0.200	0.867
0.250	0.861
0.300	0.833
0.350	0.817
0.450	0.795
0.550	0.775
0.650	0.722
0.700	0.699
0.750	0.639
0.800	0.627
0.850	0.525
0.900	0.444
0.905	0.410
0.910	0.425

times becomes weaker with decreasing density, and finally it turns into normal diffusion.

In order to examine the subdiffusive behavior more closely, we have taken a look at the trajectory of a single particle in the course of a simulation run. Figure 2 shows the distance $\Delta r(t)$ of a tagged dimer from the starting position at $t = 0$ for two values of density $\rho_0 = 0.65$ and 0.90. Upon analyzing the dimers trajectories, we find that a dimer spends most of its time confined in a well-defined area, oscillating with an amplitude typically of the order of a few lattice constants. Sometimes a dimer escapes during rare and brief events. This corresponds to the well-known cage effect observed in supercooled liquids [29–31], dense colloidal systems [3,32], and granular fluids [33–35]. At short times, particles are temporarily trapped in cages formed by their neighbors, and as a consequence, the collisions within the cage result in a time dependence of the MSD that is slower than the one in the regime of normal
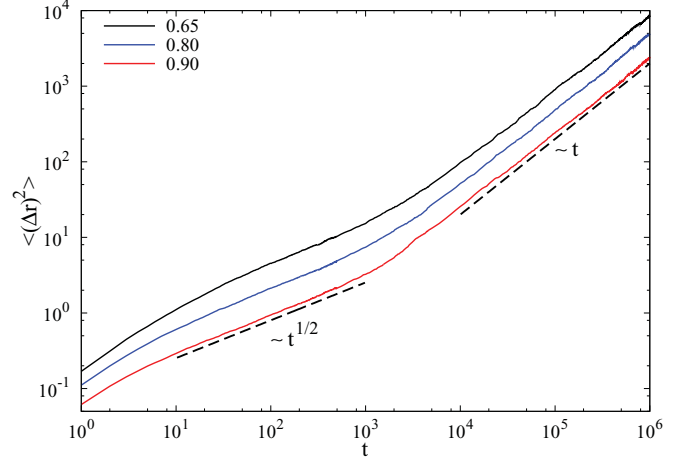
FIG. 3. (Color online) Temporal evolution of the MSD under the single-file condition for dimers at densities $\rho_0 = 0.65$, 0.80, 0.90, from top to bottom. The dashed line with slope 1 illustrates the normal diffusion, and the dashed line with slope $1/2$ describes the SFD.

diffusion. At long times, particles diffuse from cage to cage, and their movement is then less and less influenced by the effect of trapping, so that the exponent α in Eq. (2) increases ($\alpha \rightarrow 1$). In the present case escaping from the cage is achieved by cooperative motions between neighboring particles, as in the case of dense liquids or colloids.

In addition we compare the results found in the case of mutually intersecting single-file systems with those obtained for the single-file diffusion. For this purpose we prepare the appropriate initial random state of the lattice by inserting dimers in only one direction up to the chosen coverage fraction ρ_0. Furthermore, we forbid rotations of dimers (only glide moves are allowed), so that dimers diffuse along straight lines. The results for MSD as a function of time for several different densities are shown in Fig. 3. As can be seen, for all densities the initial fast grow of the MSD is followed by the pronounced $\propto t^{1/2}$ "long-time" region gradually changing to $\propto t$ asymptotic behavior. Comparison of Fig. 3 with Fig. 1 reveals that the mutual correlation in the movement of dimers due to the crossing of the arrays of lines ("channels") can strongly alter the single-file diffusion process. Indeed, in the case of mutually intersecting single-file systems, some lattice points in the channel along one specific direction can be occupied by particles moving along the other directions. As a consequence, the single filing constraint is relaxed in such a system, so that particle diffusivity may be enhanced in comparison with systems where the mutual particle exchange between the channels is excluded.

The simulations described above were augmented by additional simulations that were carried out to explore the dependence of the diffusive dynamics on the number of segments of k-mers. In Fig. 4 we compare the temporal evolution of the MSD at various densities for the two linear segments (k-mers) covering $k = 3$ and 4 lattice sites. As expected, the self-diffusion coefficient D_s is higher for the shorter objects at the same density. The MSD of 3-mers exceeds the MSD of the larger objects ($k = 4$) at intermediate and large times. This is a consequence of the fact that unlike
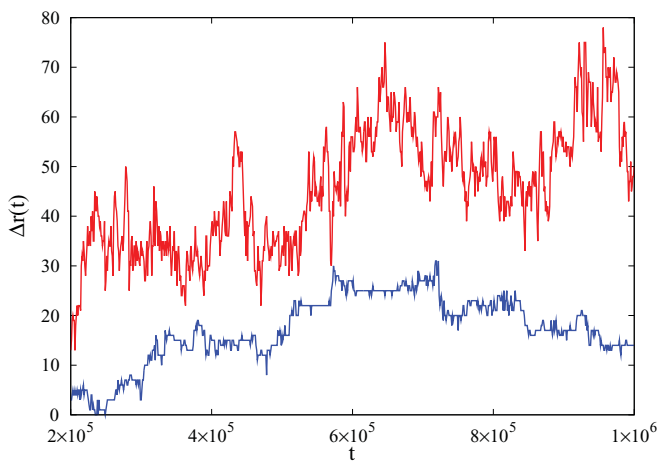
FIG. 2. (Color online) Typical time evolution of the displacement $\Delta r(t)$ of a single dimer at $\rho_0 = 0.90$ (blue, bottom curve) and $\rho_0 = 0.65$ (red, upper curve).
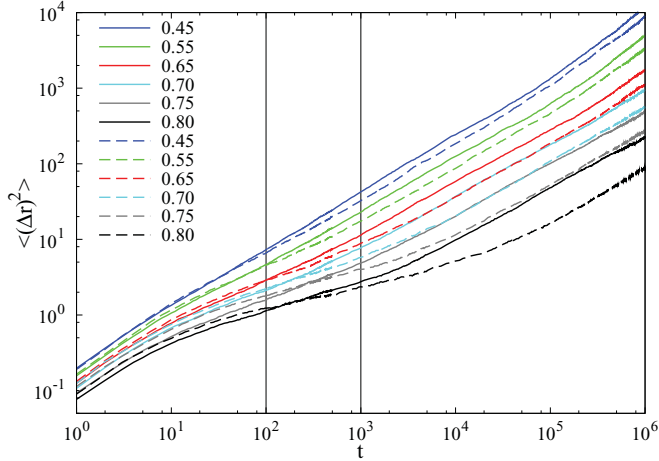
FIG. 4. (Color online) Shown here is the double logarithmic plot of the temporal evolution of the MSD for $k = 3$ (solid lines) and $k = 4$ (dashed lines) at various densities ρ_0. The solid and dashed lines represent the MSD vs time t for densities $\rho_0 = 0.45, 0.55, 0.65, 0.70, 0.75, 0.80$, from top to bottom. The values of exponent α [Eq. (2)] reported in Table II are obtained from the slopes of the MSD vs t curves in the time region between the thin vertical lines.

for the long k-mers, more possible places for displacement are allowed for short k-mers diffusing in the crossed single-file systems. Moreover, from Fig. 4 it is evident that the region of anomalous diffusion increases with the length of k-mers. The values of exponent α Eq. (2) for $k = 3, 4$ obtained from the slopes of the MSD versus t curves in the range $t \in [10^2, 10^3]$ are reported in Table II. Comparing the results from Tables I and II we can see that the exponent α decreases with the length of the k-mer for all the densities considered. Due to the fact that the dynamics of an object moving on a lattice is dictated by the geometric exclusion effects, the subdiffusion at intermediate times becomes stronger with increasing the objects' size for the same density.

We have also considered another series of numerical experiments where both rotations ($P_{\rm rot} > 0$) and glides of dimers are allowed simultaneously. In the main panel of Fig. 5 the MSD is shown in the case of density $\rho_0 = 0.90$ and for different rotation probabilities $P_{\rm rot}$. At high values of $P_{\rm rot}$, short initial transient goes over immediately into a diffusive behavior, i.e., $\langle \Delta r^2(t) \rangle = 4D_s t$. For low rotation probabilities these two regimes are separated by a time regime where the motion of dimers seems to be partially frozen so that

TABLE II. Values of the parameter α [Eq. (2)] for $k = 3, 4$ obtained from the fit to the power law (2) of the MSD in the range $t \in [10^2, 10^3]$ for various densities ρ_0.

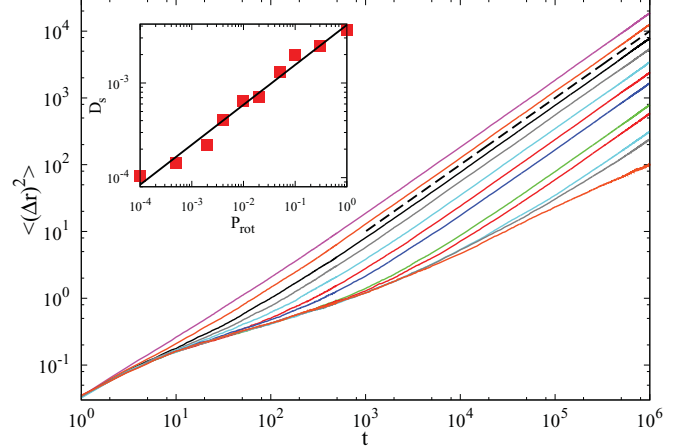| ρ_0	$\alpha(k = 3)$	$\alpha(k = 4)$
0.45	0.756	0.675
0.55	0.685	0.564
0.65	0.591	0.480
0.70	0.565	0.394
0.75	0.489	0.351
0.80	0.391	0.275

FIG. 5. (Color online) Shown here is the double logarithmic plot of the temporal evolution of the MSD for dimers in the case of $\rho_0 = 0.90$ and for various rotation probabilities $P_{\rm rot}$. The solid lines represent the MSD vs time t for probabilities $P_{\rm rot} = 1.0, 0.3, 0.1, 0.05, 0.02, 0.01, 5 \times 10^{-3}, 10^{-3}, 5 \times 10^{-4}, 10^{-4}, 5 \times 10^{-5}, 0$, from top to bottom. The dashed straight line is shown, indicating the late-time diffusive behavior, $\langle \Delta r^2(t) \rangle = 4D_s t$. Inset: the self-diffusion coefficient D_s for dimers as a function of the rotation probability $P_{\rm rot}$. The solid straight line is the power-law fit, $D_s \propto P_{\rm rot}^{0.42}$.

the slope of MSD is less than one. Accordingly, the system becomes subdiffusive, i.e., $\langle \Delta r^2(t) \rangle \propto t^\alpha$ with $\alpha < 1$, over an intermediate time window that becomes broader as $P_{\rm rot}$ decreases. It is observed that the self-diffusion coefficient D_s for $\rho_0 = 0.90$ increases with the rotation probability $P_{\rm rot}$ as shown in the inset of Fig. 5. Furthermore, for the fixed value of $P_{\rm rot}$, the dimer self-diffusion coefficient D_s decreases algebraically with the dimer density ρ_0. We omit a further discussion of these quantities as they have been presented at length elsewhere for similar models [36–38].

B. Van Hove space-time self-correlation function

We now turn our attention to a closer analysis of the motion of k-mers in the case of mutually intersecting single-file systems. We have calculated the self-part of the van Hove correlation function from the particle trajectories obtained in the simulations. Assuming an isotropic behavior, this function is given by

$$G_s(r,t) = \frac{1}{N} \left\langle \sum_{i=1}^{N} \delta(r - |\vec{r}_i(t) - \vec{r}_i(0)|) \right\rangle, \qquad (3)$$

where $\delta(\cdot)$ is the δ function, N is the number of particles, and $\vec{r}_i$ is the position vector of the ith particle. The function $G_s(r,t)$ measures the probability that a given particle has undergone a displacement r in a time interval of duration t. If the motion of particles is diffusive, then the self-part of the van Hove correlation function is Gaussian, $G_s(r,t) \propto \exp[-r^2/(4D_s t)]$, where D_s is the self-diffusion coefficient [39]. In the following, attention will be restricted to the case in which the rotation of k-mers is explicitly forbidden; only the glide moves are allowed.
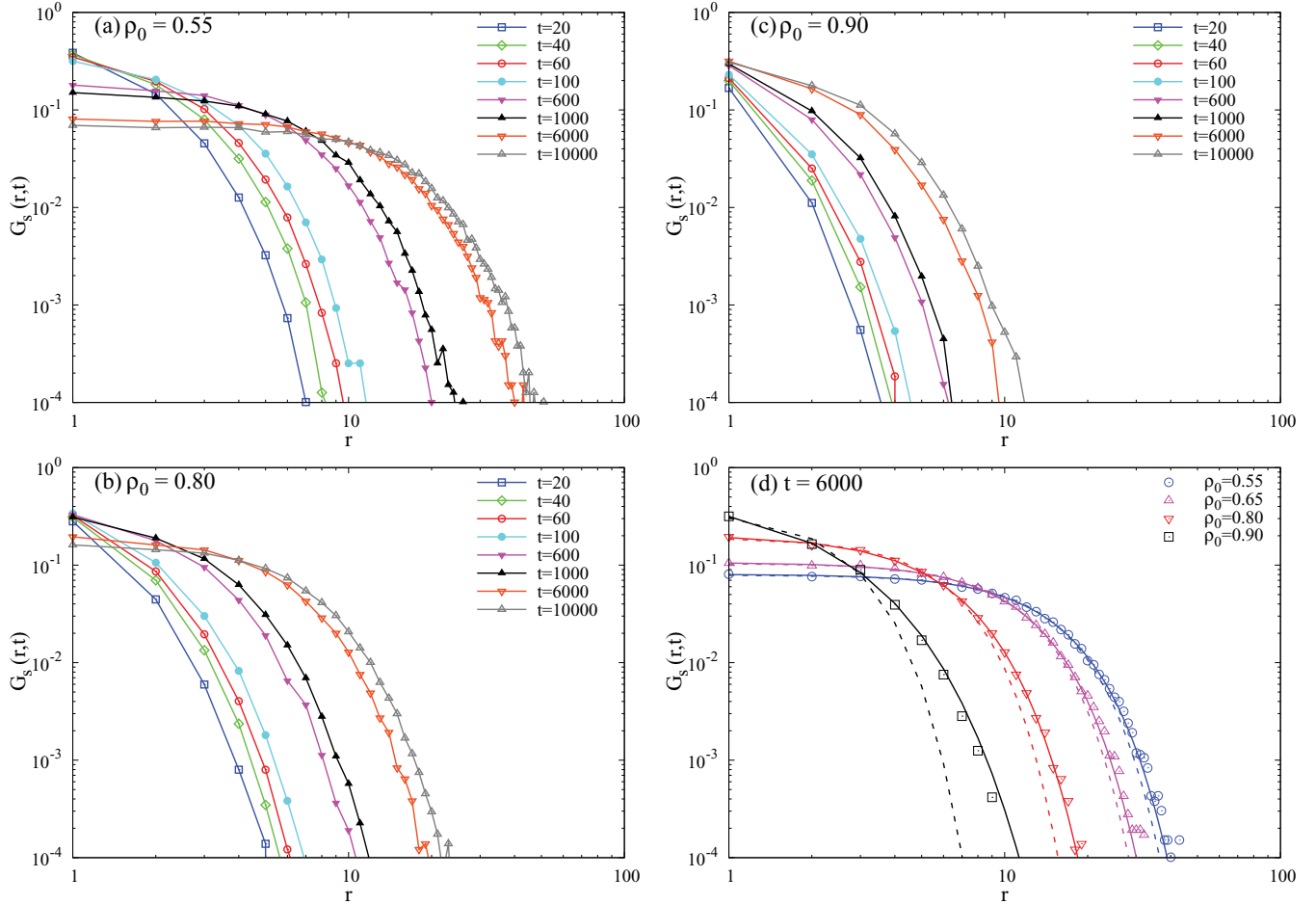
FIG. 6. (Color online) Self-part of the van Hove correlation function $G_s(r,t)$ of dimers for different densities: $\rho_0 = 0.55$ (a), $\rho_0 = 0.80$(b), and $\rho_0 = 0.90$(c). The curves in each graph correspond to various times ranging from $t = 20$ to 10^4 as indicated in the legend. The symbols are the actual data and the lines are just a guide for the eye. In (d) the data correspond to four different densities ρ_0 (see legend) and time $t = 6000$. The dashed lines are the Gaussian fitting functions, $G_s(r,t) = [\alpha(t)/\pi] \exp[-\alpha(t)r^2]$, and the solid lines are the stretched exponential fits (4). Distances on the horizontal axis are measured in lattice spacing units.

First, let us consider the dynamical properties of dimers for different coverage fractions. In Fig. 6, we have plotted $G_s(r,t)$ for three densities: $\rho_0 = 0.55$ (a), 0.80 (b), and 0.90 (c) at different times ranging from $t = 20$ to $t = 10^4$. We can clearly see that at low density [Fig. 6 (a)] $G_s(r,t)$ decays in a regular way; e.g., it is localized at short distances (typically $r < 10$) for short times and tends to delocalize for large times. This changes slightly for intermediate densities [Fig. 6 (b)]. Here we see that for times in the range $20 \leqslant t \leqslant 10^3$ the curves show a weak tendency to cluster for $1 \leqslant r \leqslant 10$. This effect is much more pronounced at the highest density investigated [Fig. 6 (c)], where it can be observed for times in the range $20 \leqslant t \leqslant 10^4$. This clustering is the signature that the movement of the particles has drastically slowed at such densities. We note that this slowing takes place for distances of a few lattice constants; thus the particle still remains in the cage formed by the particles that surrounded it at the zero time.

In Fig. 6 (d) we have plotted $G_s(r,t)$ for four different coverage fractions ranging from 0.55 to 0.90 at the fixed time $t = 6000$. The single particle motion at timescales corresponding to $t = 6000$ is subdiffusive for all the densities considered (see Fig. 1). It can be easily seen that, especially

for large densities, there is a pronounced deviation of $G_s(r,t)$ from Gaussian distribution, shown as dashed lines. The small r behavior, however, is not far from the Gaussian approximation, corresponding to the motion of most of the particles around their initial position. Additionally, a small fraction of the particles find pathways to explore larger distances during the observational time and contributing to the tail of $G_s(r,t)$.

In Fig. 7 the spatial dependence of $G_s(r,t)$ for various k-mers is displayed for the fixed time $t = 6000$, and for different values of density: $\rho_0 = 0.65$, 0.80. With increasing length of the k-mers, the width of $G_s(r,t)$ decreases noticeably for both densities. Additional simulations performed at various times confirmed that the change in the shape of $G_s(r,t)$ over k becomes more pronounced as t increases, for all densities. The observed differences in the dynamics of the larger and the smaller particles diffusing in the crossed single-file systems can be explained as follows. Since dimers are smaller than the other k-mers, they are more mobile, as can also be recognized from the fact that the diffusion coefficient for dimers is larger than the one for the longer k-mers (see Figs. 1 and 4). Consequently, dimers are able to make some movements (jumps) that the longer objects cannot do.
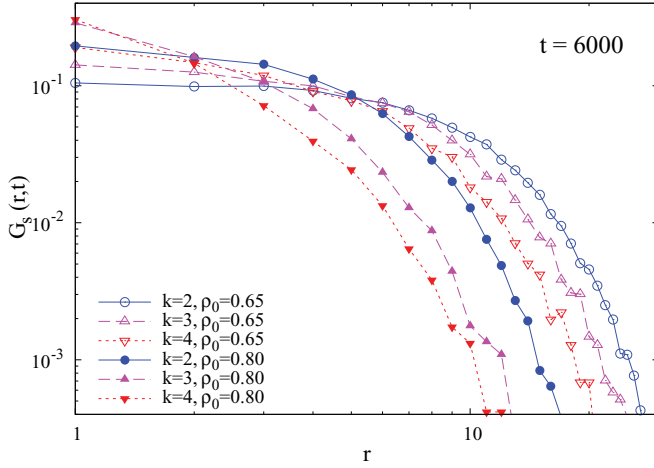
FIG. 7. (Color online) Spatial dependence of the self-part of the van Hove correlation function $G_s(r,t)$ for $k = 2$ (circles), $k = 3$ (up triangles), and $k = 4$ (down triangles). The symbols are the actual data, and the lines are just a guide for the eye. The data correspond to densities $\rho_0 = 0.65$ (empty symbols) and 0.80 (full symbols) and time $t = 6000$. Distances on the horizontal axis are measured in lattice spacing units.

In order to provide the best analytical approximation for the self-part of the van Hove correlation function $G_s(r,t)$, we examined a wide set of phenomenological fitting functions for relaxation processes in many complex disordered systems [40]. Several attempts have been previously made to empirically fit the non-Gaussian shape of $G_s(r,t)$ with known functional forms. In order to characterize the dynamical heterogeneity in a model for permanent gels, Abete *et al.* [41] have tried to fit their numerically determined $G_s(r,t)$ with the sum of two and more different Gaussian functions. Gao and Kilfoil [42] have also recognized that near the colloid-gel transition $G_s(r,t)$ has a bimodal Gaussian form. Basing their analysis on the experimentally measured $G_s(r,t)$, Weeks *et al.* [43] obtained that $G_s(r,t)$ is probably better fitted with a stretched exponential function. Recently it has been shown [25] that $G_s(r,t)$ for a broad class of materials close to glass and jamming transition are better represented by a superposition of a central Gaussian along with an exponential tail for the large distances. However, the best agreement with our simulation data was obtained by the stretched exponential function. The fitting function we have used is of the form

$$G_s(r,t) = B(t) \exp \left\{ - \left[\frac{r}{\lambda(t)} \right]^{\beta(t)} \right\}. \qquad (4)$$

The solid lines through the data in Fig. 6(d) are fits to Eq. (4). In the case of dimers, the fitting parameters $\lambda(t)$ and $\beta(t)$ are given in Fig. 8 and for four values of density, $\rho_0 = 0.55, 0.65, 0.80, 0.90$. It is noteworthy that for all densities ρ_0, the parameter $\lambda(t)$ seems to be a simple power law of time:

$$\lambda(t) = K\, t^\gamma. \qquad (5)$$

The values of the exponent γ obtained for the densities below $\rho_0 = 0.85$ are in the range from 0.36 to 0.40; for $\rho_0 = 0.90$, we obtained the value of $\gamma = 0.23$. The parameter λ is also sensitive to the variations of object size. The inset of Fig. 8(a)
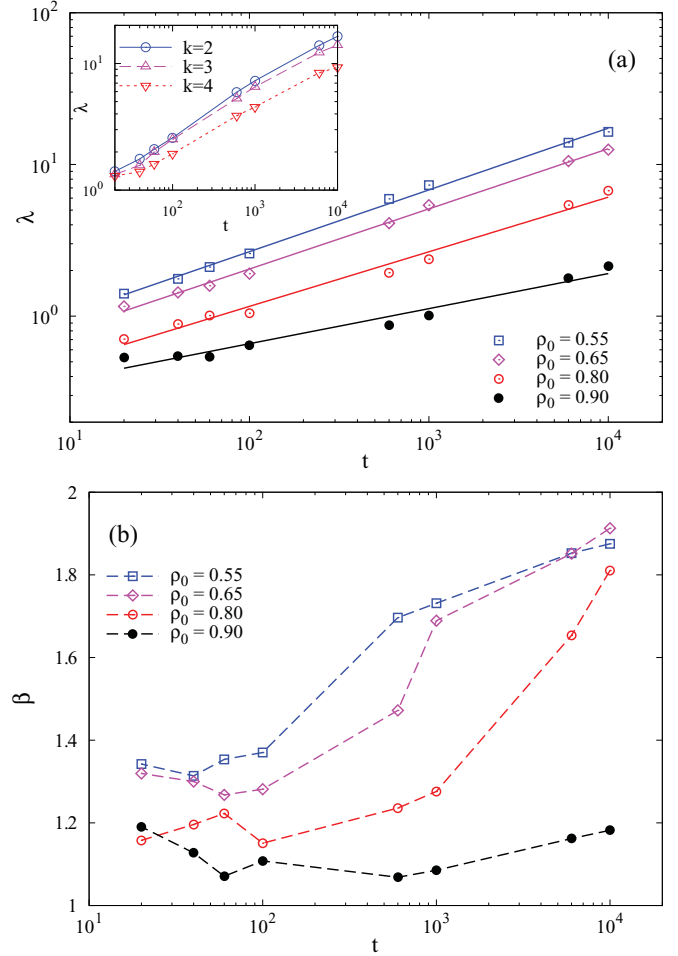

FIG. 8. (Color online) Main figure: The parameters $\lambda(t)$ (a) and $\beta(t)$ (b), obtained by the stretched exponential fit [Eq. (4)] for the case of dimers, as a function of time t. The symbols correspond to densities $\rho_0 = 0.55, 0.65, 0.80, 0.90$ as indicated in the legend. In the main panel of (a) the solid lines are the power-law fits of Eq. (5). Inset in (a): Parameter $\lambda(t)$ of the stretched exponential fit [Eq. (4)] vs time for the cases of $k = 2, 3, 4$. All results are for density $\rho_0 = 0.55$.

compares the time evolution of the fitting parameter $\lambda(t)$ for three k-mers ($k = 2, 3, 4$) and for density $\rho_0 = 0.55$. The size dependence of the parameter $\lambda(t)$ occurs already at early times. As is expected, for cooperative diffusion with geometrical constraints [19], parameter λ, i.e., the characteristic width of the van Hove correlation function $G_s(r,t)$, decreases with increasing k.

As shown in Fig. 8(b), the values of the fitting parameter $\beta(t)$ [Eq. (4)] ranges between 1 and 2 for all densities ρ_0. As may be expected, however, and consistent with the MSD behavior seen in Fig. 1, the parameter β reaches a value close to 2 for large times and for sufficiently low densities. This reflects the fact that the spatial dependence of $G_s(r,t)$ exhibits a clear trend to transform from the exponential behavior at small times to the Gaussian form at long times. In the case of mutually intersecting arrays of single-file systems, the stretched exponential function (4) therefore allows one to describe the self-part of the van Hove correlation function $G_s(r,t)$ at different times without changing the fitting formula.

C. Intermediate scattering function

In this section we study the single-particle density fluctuation dynamics of our model. Relevant information on the relaxation dynamics over different length scales is embedded in the self-intermediate scattering function (SISF) defined as

$$F_s(\vec{q},t) = \frac{1}{N} \left\langle \sum_{i=1}^{N} \exp\{i\vec{q} \cdot [\vec{r}_i(t) - \vec{r}_i(0)]\} \right\rangle, \quad (6)$$

where, again, $\vec{r}_i(t)$ is the position of the ith particle in units of the lattice constant. The wave vector $\vec{q}$ can take the discrete values $\vec{q} = (2\pi/L)\vec{n}$, where $\vec{n} = (n_x, n_y)$ has integer components n_x and n_y ranging from 0 to $L/2 = 30$.

Let us first consider the case of dimers when the rotation moves can never occur (i.e., $P_{\rm rot} = 0$ and $P_{gl} = 1$). Figure 9 presents our numerical results for the self-intermediate scattering function $F_s(q_n,t)$ at various densities ρ_0 and for various wave vectors. We choose $\vec{q} = (q_n, 0)$, where $q_n = (2\pi/L)n$ and $n = 1, 2, 4, 6, 8, 10, 15, 20, 25, 30$. At low densities $\rho_0 < 0.60$ [see, e.g., Fig. 9(a)] all the curves decay to zero; i.e., the length of all the simulations allows

the fluctuations to become completely uncorrelated. As can be seen, for all densities $F_s(q_n,t)$ decays more slowly the smaller q_n is. In the case of the highest density investigated, $\rho_0 = 0.90$ [Fig. 9(c)]; due to the very slow dynamical relaxation, at small values of the wave vector q_n ($n \leqslant 6$), only a part of the $F_s(q_n,t)$ can be observed.

We do not observe a plateau in the decrease of $F_s(q_n,t)$ in contrast to what is often reported for colloids and glasses. In dense colloids and supercooled liquids, $F_s(q_n,t)$ shows the two-step relaxation behavior: (1) the fast β relaxation that corresponds to the diffusion inside the cage, followed by (2) the α relaxation corresponding to the time it takes for the particle to diffuse out of the cage. Instead, in our model the $F_s(q_n,t)$ curves stay close to unity for a time span that increases with increasing density [see, e.g., Fig. 9(d)]. Similar behavior has also been observed in the Kob-Andersen kinetic lattice gas model, kinetically constrained spin models, and sheared granular materials close to the jamming transition [36,44,45]. A simple explanation of the absence of a plateau can be obtained via the following argument. When a particle in a real fluid is temporarily caged by its surroundings, it can
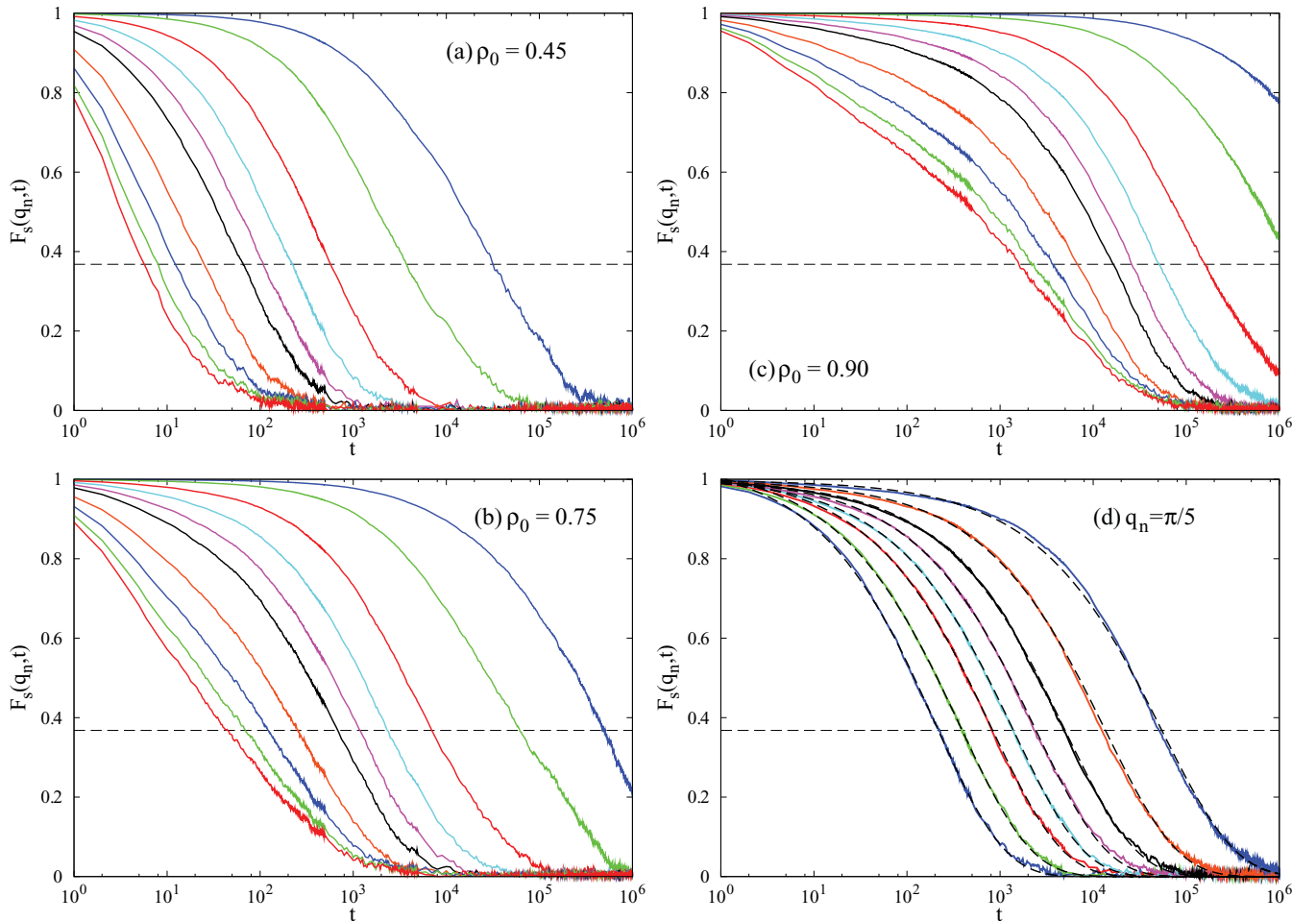

FIG. 9. (Color online) The time dependence of the SISF, $F_s(q_n,t)$, for dimers for different densities: $\rho_0 = 0.45$(a), $\rho_0 = 0.75$(b), and $\rho_0 = 0.90$(c). The curves in graphs (a)–(c) correspond to the wave vectors $\vec{q} = (q_n, 0)$, where $q_n = (2\pi/L)n$ and $n = 30, 25, 20, 15, 10, 8, 6, 4, 2, 1$ (from left to right). In (d) the solid curves correspond to the SISF, $F_s(q_n,t)$, of dimers for densities $\rho_0 = 0.45, 0.55, 0.65, 0.70, 0.75, 0.80, 0.85, 0.90$ (from left to right), and for the wave vector $q_n = \pi/5$, ($n = 6$). The dashed curves are the stretched exponential fits of Eq. (7), with the parameters τ and α given in Fig. 10. The horizontal dashed line indicates the $1/e$ value.

nevertheless rattle in its cage, and hence the SISF decays on a relatively short time scale to a plateau value. Only for much larger times the particles are able to leave their cages, and hence the SISF starts to decay to zero. In our model almost all caged particles are immobile until their cages fall apart. The absence of the rattling motion causes that the value of the plateau is unity or very close to it. Thus the early-time β regime would be very difficult or impossible to observe.

In Fig. 9(d) we show $F_s(q_n,t)$ for nearly all densities ρ_0 investigated for one particular wave vector $q_n = \pi/5$ ($n = 6$). Analyzing the curves in Fig. 9(d) we find that the decreasing of $F_s(q_n,t)$ is slower than exponential in time. In addition, the curves for different values of density are very similar in form. We have fitted the slow decay of $F_s(q_n,t)$ to the Kohlrausch-Williams-Watts (KWW) or stretched exponential function

$$F_s(q_n,t) = A \exp\left\{-\left[\frac{t}{\tau(q_n)}\right]^{\alpha(q_n)}\right\}, \qquad (7)$$

where $\alpha(q_n)$ is the parameter measuring the deviation from the single exponential form ($0 < \alpha \leqslant 1$) and $\tau(q_n)$ is the relaxation time. Fits of this stretched exponential form to
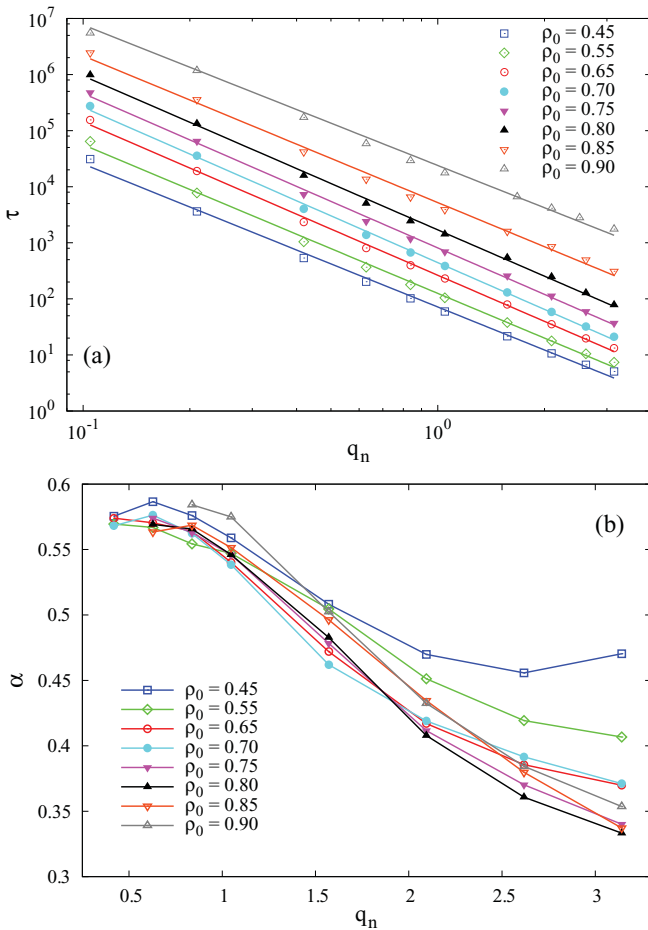

FIG. 10. (Color online) The parameters $\tau(q_n)$ (a) and $\alpha(q_n)$ (b), obtained by the stretched exponential fits of Eq. (7) for the case of dimers, as a function of the wave vector q_n. The symbols correspond to densities $\rho_0 = 0.45, 0.55, 0.65, 0.70, 0.75, 0.80, 0.85, 0.90$ as indicated in the legend. The solid lines in (a) are the power-law fits of Eq. (8).

the simulation data are shown as dashed lines in Fig. 9(d). Since the fitting parameter A is approximately equal to unity for all wave vectors and densities, the wave-dependent relaxation time $\tau(q_n)$ can be defined as the time it takes for the simulation curves of $F_s(q_n,t)$ to fall to the level of $1/e$, i.e., $F_s(q_n,\tau) = 1/e$.

We now focus on the q_n dependence of both the relaxation time $\tau(q_n)$ [Fig. 10(a)] and the exponent $\alpha(q_n)$ [Fig. 10(b)], for various values of the density ρ_0. It is noteworthy that for all densities ρ_0, the parameter $\tau(q_n)$ seems to be a simple power law of the wave vector:

$$\tau(q_n; \rho_0) = R(\rho_0)\, q_n^{-\delta}, \qquad (8)$$

with the same exponent $\delta = 2.70 \pm 0.07$ for all ρ_0. On the other hand, the stretching exponent $\alpha(q_n)$ has the values noticeably below one [Fig. 10(b)] and decreases progressively below 0.5 for higher densities. The obtained values of $\alpha(q_n)$, different from unity, confirm the nonexponential relaxation of $F_s(q_n,t)$, which can be attributed to the presence of dynamic heterogeneities due to caging [24]. For small values of q_n the exponent $\alpha(q_n)$ is rather weakly dependent on the density ρ_0. This provides the collapse of correlators onto a single curve when the time is scaled as $t/\tau(q_n)$. Figure 11 shows the time-density superposition of the correlators $F_s(q_n,t)$ in the case of dimers for all densities ρ_0 investigated. For large wave vectors q_n (small length scale) the exponent $\alpha(q_n)$ depends on the density [see Fig. 10(b)]. Thus the time-density superposition principle does not hold, likely because the short time dynamical process can induce a significant relaxation on the small length scales.

Finally, we consider the behavior of the relaxation time τ as a function of the density ρ_0. We have found that the slowing of the dynamics with ρ_0 is consistent with a scaling law

$$\frac{1}{\tau(q_n; \rho_0)} = S(q_n)\,(\rho_c - \rho_0)^{\varkappa}. \qquad (9)$$

We have performed a three-parameter fitting of our simulation data for $\tau(q_n; \rho_0)$ to obtain the parameters $\varkappa$, ρ_c, and $S(q_n)$. In Fig. 12 the inverse relaxation time τ^{-1} is presented for the case
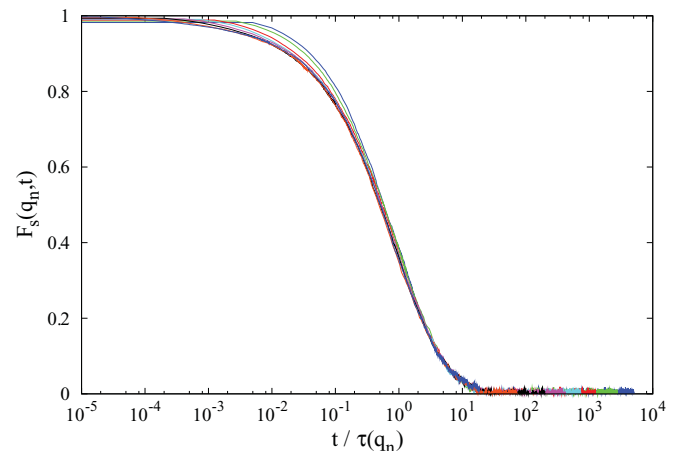

FIG. 11. (Color online) The SISF, $F_s(q_n,t)$, at $n = 6$ ($q_n = \pi/5$) rescaled to $t/\tau(q_n)$, for dimers at densities $\rho_0 = 0.45, 0.55, 0.65, 0.70, 0.75, 0.80, 0.85, 0.90$. All the curves verify the time-density superposition principle.
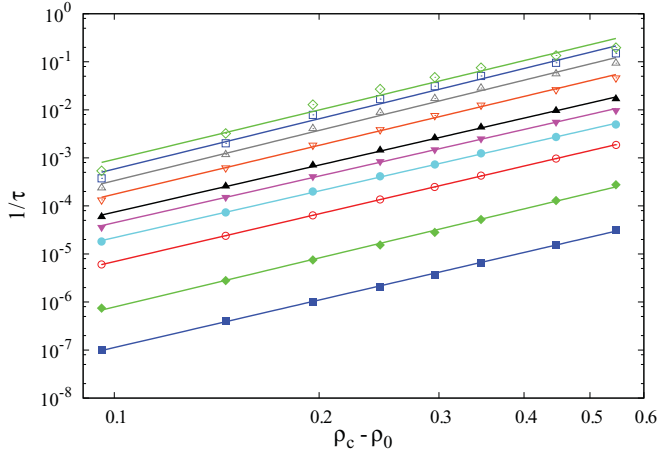
FIG. 12. (Color online) The inverse relaxation time, $1/\tau$, extracted from the SISF of dimers, as a function of $\rho_c - \rho_0$, where $\rho_c = 0.9958 \pm 0.016$. The symbols correspond to the wave vectors $\vec{q} = (q_n, 0)$, where $q_n = (2\pi/L)n$ and $n = 30, 25, 20, 15, 10, 8, 6, 4, 2, 1$ (from top to bottom). The solid lines are the power-law fits of Eq. (9).

of dimers as a function of $\rho_c - \rho_0$ for different wave vectors. The final value of $\rho_c = 0.9958 \pm 0.016$, used in Fig. 12, was calculated as the average value for all wave vectors studied. The linear trends in Fig. 12 show the power-law behavior as given by Eq. (9) in the entire range of densities considered, with the same exponent $\varkappa = 3.34 \pm 0.12$ for all wave vectors. This functional dependence of relaxation has also been found in many numerical lattice gas models [17,36,46]. It is important to stress that the density ρ_c is approximately equal to the density of closest packing of dimers on the 2D triangular lattice. Indeed, when the deposited dimers are subject to diffusion, the coverage fraction approaches the closest packing limit $\theta_{CPL} \lesssim 1$ [47–49], because the diffusion allows the formation of gaps within which a fraction of deposition attempts can succeed. This would suggest that there is no critical density lower than the closest packing limit at which a structural arrest of the system occurs.

An important prediction of the mode coupling theory is the existence of power-law divergences for both the time scale τ and the inverse of the self-diffusion coefficient D_s, with the same exponent in both cases. We have calculated the diffusion coefficient from the MSD at very long times. The values obtained for D_s in the case of dimers are well fitted by a power law $D_s \propto (\rho_c - \rho_0)^{\varkappa_1}$ with $\rho_c = 0.996$ and $\varkappa_1 = 3.33$. As shown in Fig. 13, our simulation results confirm a power law for the self-diffusion coefficient D_s, with the same exponent (within errors) as for the time scale.

Returning to the case of simulations where both rotations and glides of dimers are allowed, we obtain that for high rotation probabilities $P_{rot} \lesssim 1$, $F_s(q_n, t)$ shows a simple exponential profile at all wave vectors. As P_{rot} decreases, the $F_s(q_n, t)$ curves become more and more stretched exponential. These results are displayed in Fig. 14 for intermediate value of $q_n = \pi/5$ ($n = 6$) and for density $\rho_0 = 0.90$. For all rotation probabilities P_{rot} the whole time interval of $F_s(q_n, t)$ can be fitted by a stretched exponential function [Eq. (7)], where the exponent $\alpha(q_n)$ depends on the probability P_{rot}. We extract the
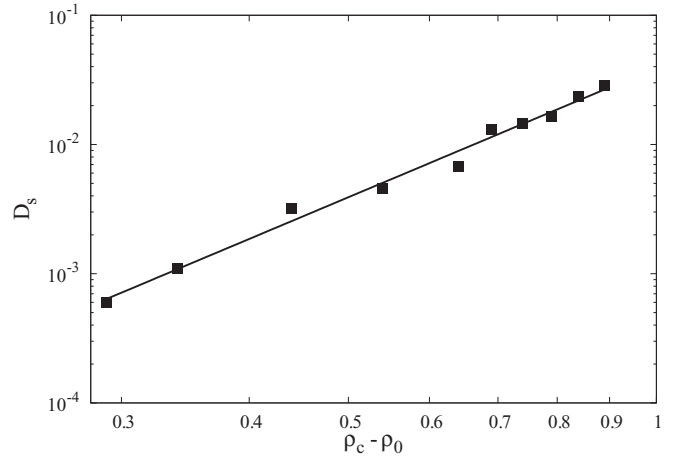

FIG. 13. The self-diffusion coefficient D_s of dimers, as a function of $\rho_c - \rho_0$, where $\rho_c = 0.996$. The straight line is the power-law $D_s \propto (\rho_c - \rho_0)^{\varkappa_1}$ with $\varkappa_1 = 3.33$.

time scales $\tau(q_n)$ from the scattering function in the usual way, $F_s(q_n, \tau) = 1/e$. According to Fig. 15(a), $\tau(q_n)$ decreases very rapidly with increasing rotation probability P_{rot}. In Fig. 15(b) we show the exponent $\alpha(q_n)$ as a function of the wave vector for various rotation probabilities P_{rot}. For sufficiently high values of P_{rot} and for small q_n (i.e., large length scales) we obtain that the relaxation time $\tau(q_n)$ scales as q_n^{-2} and $\alpha(q_n) \rightarrow 1$. Hence, at high P_{rot} dimers perform a normal diffusive motion on large length and time scales, and therefore $F_s(q_n, t) \propto \exp(-D_s q_n^2 t)$ for small q_n and large t.

Finally, we investigated the dependence of SISF, $F_s(q_n, t)$, on the length of k-mers. In Fig. 16 we compare the decay of $F_s(q_n, t)$ at density $\rho_0 = 0.55$ for the two k-mers: $k = 3$ and $k = 4$. We see that for small wave vectors q_n (long wavelengths) correlator $F_s(q_n, t)$ decays more slowly for the longer k-mer. However, the relaxation behavior of correlators $F_s(q_n, t)$ that probe the system on the length scale of
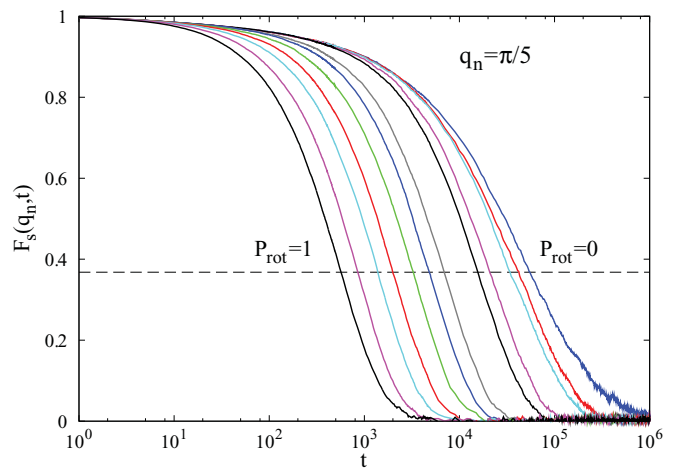

FIG. 14. (Color online) The time dependence of the SISF, $F_s(q_n, t)$, for density $\rho_0 = 0.90$, and for the wave vector $q_n = \pi/5$, ($n = 6$). The solid curves correspond to $F_s(q_n, t)$ for rotation probabilities $P_{rot} = 1.0, 0.3, 0.1, 0.05, 0.02, 0.01, 5 \times 10^{-3}, 10^{-3}, 5 \times 10^{-4}, 10^{-4}, 5 \times 10^{-5}, 0$, from left to right. The horizontal dashed line indicates the $1/e$ value.
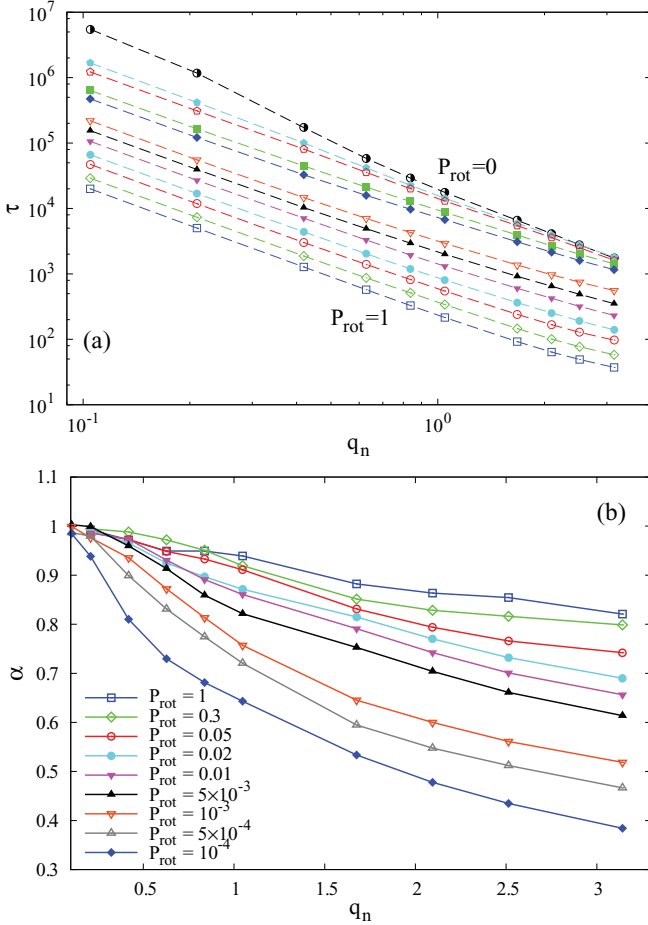
FIG. 15. (Color online) The parameters $\tau(q_n)$ (a) and $\alpha(q_n)$ (b), obtained by the stretched exponential fits of Eq. (7) for the case where both rotations and glides of dimers are allowed. The symbols are the actual data and the lines are just a guide for the eye. In (a) the lines represent the τ vs q_n dependence for probabilities $P_{rot} = 0$, 5×10^{-5}, 10^{-4}, 5×10^{-4}, 10^{-3}, 5×10^{-3}, 0.01, 0.02, 0.05, 0.1, 0.3, 1.0, from top to bottom. In (b) the symbols correspond to various probabilities $P_{rot} \geqslant 10^{-4}$ as indicated in the legend. All the results are for density $\rho_0 = 0.90$.

typical interparticle distances, i.e., for large values of q_n, is independent of the length of k-mers for all times. For other densities we get qualitatively the same results. A consequence of these outcomes is that the relaxation time $\tau(q_n)$ for small wave vectors q_n increases with the length of the k-mer (see Fig. 17). We also found that the relaxation time $\tau(q_n)$ can be well fitted by a power-law behavior [Eq. (8)] for all the k-mers investigated. When length of k-mer increases, this power-law behavior is restricted to smaller and smaller q_n. Furthermore, the relaxation times $\tau(q_n)$ for the largest values of q_n have very similar values for all k-mers (see Fig. 17), which is in accord with the previously stated fact that the correlator $F_s(q_n,t)$ becomes k-independent with increasing q_n.

IV. CONCLUDING REMARKS

The model investigated in this work is a two-dimensional lattice gas model, where the interactions originate from
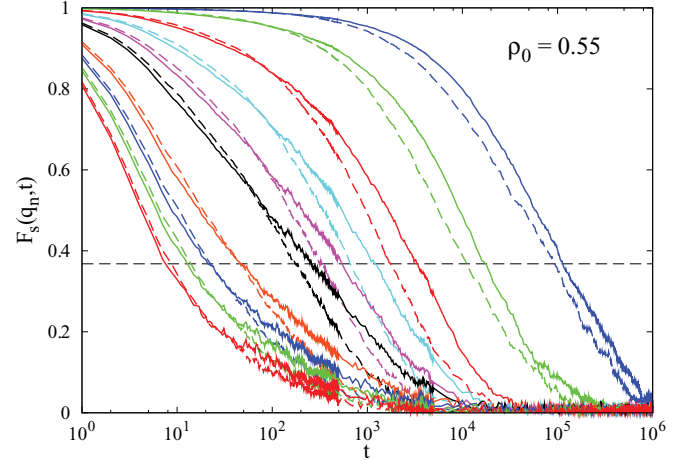

FIG. 16. (Color online) The time dependence of the SISF, $F_s(q_n,t)$, at density $\rho_0 = 0.55$ for $k = 3$ (dashed lines), and $k = 4$ (solid lines). The solid (dashed) curves correspond to wave vectors $\vec{q} = (q_n,0)$, where $q_n = (2\pi/L)n$ and $n = 30, 24, 20, 16, 10, 8, 6, 4, 2, 1$ (from left to right). The horizontal dashed line indicates the $1/e$ value.

the excluded volume. As a consequence of the restrictions on particle motion, the model has the physical features associated with the cage effect in high-density liquids. We have highlighted the occurrence of very complex dynamical behavior as soon as a multitude of single-file systems are composed into channel networks.

By studying the mean-square displacement of k-mers we have found that the suppression of rotational motion results in a subdiffusive dynamics at intermediate times between the initial transient and the long-time diffusive regime. Subdiffusion stems from the trapping of the particles within the cages. Our results indicate that the mutual correlation in the movement of k-mers due to the crossing of the arrays of lines can strongly alter the single-file diffusion process. We have focused our attention on the single particle trajectories and have analyzed the self-part of the van Hove distribution function
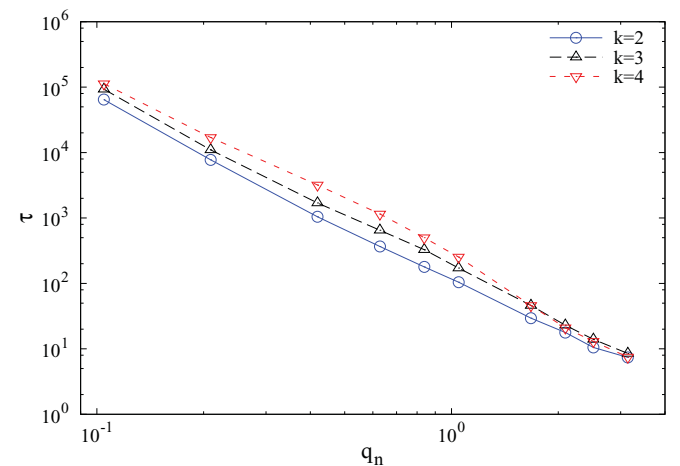

FIG. 17. (Color online) Wave-vector dependence of the relaxation times $\tau(q_n)$ [Eq. (7)] at density $\rho_0 = 0.55$ for various k-mers: $k = 2$ (circles), $k = 3$ (up triangles), and $k = 4$ (down triangles).

$G_s(r,t)$ in detail. We have shown that there is a pronounced deviation of $G_s(r,t)$ from the Gaussian distribution, especially at high densities. It was obtained that the stretched exponential function (4) excellently describes the spatial decay of $G_s(r,t)$ at intermediate times. Since the stretching exponent β for all densities ranges between 1 and 2, the spatial dependence of $G_s(r,t)$ interpolates between the initial exponential form and the long-time Gaussian behavior.

Dynamical behavior of the self-intermediate scattering function $F_s(q_n,t)$ has also been investigated. We have found that the decay of $F_s(q_n,t)$ to zero occurs via the Kohlrausch-Williams-Watts law (7) for all values of the wave vector q_n and for all densities ρ_0. At all densities, the characteristic timescale $\tau(q_n)$ is found to decrease with the wave vector q_n according to a simple power law (8), $\tau(q_n;\rho_0) \propto q_n^{-\delta}$. The time-density superposition principle (Fig. 11) seems to hold for $F_s(q_n,t)$ for small values of q_n and for all densities. However, it seems to work well for large values of q_n and high densities. Indeed, for the large wave vectors q_n and sufficiently high densities $\rho_0 \gtrsim 0.65$, the exponent $\alpha(q_n)$ [Eq. (7)] is weakly dependent on the density ρ_0 (Fig. 10). Finally, we have considered the behavior of the relaxation time τ as a function of the density ρ_0. We have shown that for all wave vectors, relaxation times $\tau(q_n;\rho_0)$ display a power-law divergence [Eq. (9)] at densities around the closest packing limit $\theta_{CPL} \lesssim 1$ for our model. The time scale and the diffusion coefficient show qualitatively the expected behavior as a function of density, since the inverse of the self-diffusion coefficient D_s also seems to diverge with the power law at the maximum density θ_{CPL}. This suggests that there is no dynamical transition in this model; i.e., the structural arrest of the model seems to happen only at the maximum density θ_{CPL}. Due to the fact that the dynamics of an object moving on a lattice is dictated by geometric exclusion effects, the dynamical behavior of the system is severely slowed with the increase of the length of the objects.

There are several possible ways of extending the results presented here. It would be interesting to perform a similar investigation with objects of various rotational symmetries on a triangular lattice [26,27,50,51]. As an open possibility for the future, we think that a lattice diffusive model presented in this work can be generalized to mixtures of several kinds of objects. This would allow us to study the role that the polydispersity, size, and the symmetry properties of the particles play in the relaxation process of structural glass formers and granular materials.

[1] R. Metzler and J. Klafter, J. Phys. A: Math. Gen. **37**, R161 (2004).

[2] G. Drazer and D. H. Zanette, Phys. Rev. E **60**, 5858 (1999).

[3] E. R. Weeks and D. A. Weitz, Chem. Phys. **284**, 361 (2002).

[4] R. Hilfer, Chem. Phys. **284**, 399 (2002).

[5] M. Weiss, H. Hashimoto, and T. Nilsson, Biophys. J. **84**, 4043 (2003).

[6] K. Ritchie, X.-Y. Shan, J. Kondo, K. Iwasawa, T. Fujiwara, and A. Kusumi, Biophys. J. **88**, 2266 (2005).

[7] S. Zschiegner, S. Russ, R. Valiullin, M.-O. Coppens, A. J. Dammers, A. Bunde, and J. Kärger, Eur. Phys. J. Special Topics **161**, 109 (2008).

[8] K. Kim, K. Miyazaki, and S. Sato, Europhys. Lett. **88**, 36002 (2009).

[9] T. Voigtmann and J. Horbach, Phys. Rev. Lett. **103**, 205901 (2009).

[10] J. Kurzidim, D. Coslovich, and G. Kahl, Phys. Rev. Lett. **103**, 138303 (2009).

[11] V. Krakoviack, Phys. Rev. E **79**, 061501 (2009).

[12] J. Kärger and D. M. Ruthven, *Diffusion in Zeolites and Other Microporous Solids* (Wiley, New York, 1992).

[13] F. Gambale, M. Bregante, F. Stragapede, and A. M. Cantu, J. Membr. Biol. **154**, 69 (1996).

[14] J. Kärger, Phys. Rev. A **45**, 4173 (1992).

[15] C. Baerlocher, W. M. Meier, and D. H. Olson, *Atlas of Zeolite Structure Types* (Elsevier, London, 2001).

[16] A. Brzank, G. M. Schütz, P. Bräuer, and J. Kärger, Phys. Rev. E **69**, 031102 (2004).

[17] C. Fusco, P. Gallo, A. Petri, and M. Rovere, Phys. Rev. E **65**, 026127 (2002).

[18] C. Fusco, A. Fasolino, P. Gallo, A. Petri, and M. Rovere, Phys. Rev. E **66**, 031301 (2002).

[19] I. Lončarević, Z. M. Jakšić, S. B. Vrhovac, and Lj. Budinski-Petković, Eur. Phys. J. B **73**, 439 (2010).

[20] J. W. Evans, Rev. Mod. Phys. **65**, 1281 (1993).

[21] V. Privman, Colloids Surf. A **165**, 231 (2000).

[22] A. Cadilhe, N. A. M. Araújo, and V. Privman, J. Phys. Condens. Matter **19**, 065124 (2007).

[23] J. C. Phillips, Rep. Prog. Phys. **59**, 1133 (1996).

[24] M. D. Ediger, Annu. Rev. Phys. Chem. **52**, 99 (2000).

[25] P. Chaudhuri, L. Berthier, and W. Kob, Phys. Rev. Lett. **99**, 060604 (2007).

[26] Lj. Budinski-Petković and U. Kozmidis-Luburić, Phys. Rev. E **56**, 6904 (1997).

[27] Lj. Budinski-Petković, M. Petković, Z. M. Jakšić, and S. B. Vrhovac, Phys. Rev. E **72**, 046118 (2005).

[28] R. Metzler and J. Klafter, Phys. Rep. **339**, 1 (2000).

[29] J. Colmenero, F. Alvarez, and A. Arbe, Phys. Rev. E **65**, 041804 (2002).

[30] W. Kob and H. C. Andersen, Phys. Rev. E **51**, 4626 (1995).

[31] S. Mossa, R. Di Leonardo, G. Ruocco, and M. Sampoli, Phys. Rev. E **62**, 612 (2000).

[32] W. van Megen, J. Phys. Condens. Matter **14**, 7699 (2002).

[33] G. Marty and O. Dauchot, Phys. Rev. Lett. **94**, 015701 (2005).

[34] P. M. Reis, R. A. Ingale, and M. D. Shattuck, Phys. Rev. Lett. **98**, 188301 (2007).

[35] R. Candelier, O. Dauchot, and G. Biroli, Phys. Rev. Lett. **102**, 088001 (2009).

[36] W. Kob and H. C. Andersen, Phys. Rev. E **48**, 4364 (1993).

[37] J. Jäckle and A. Krönig, J. Phys.: Condens. Matter **6**, 7633 (1994).

[38] A. C. Pan, J. P. Garrahan, and D. Chandler, Phys. Rev. E **72**, 041106 (2005).

[39] J. P. Hansen and I. R. McDonald, *Theory of Simple Liquids,* 2nd ed. (Academic Press, New York, 1990)

[40] R. Hilfer, J. Non-Cryst. Solids **305**, 122 (2002).

[41] T. Abete, A. de Candia, E. Del Gado, A. Fierro, and A. Coniglio, Phys. Rev. E **78**, 041404 (2008).

[42] Y. Gao and M. L. Kilfoil, Phys. Rev. Lett. **99**, 078301 (2007).

[43] E. R. Weeks, J. C. Crocker, A. C. Levitt, A. Schofield, and D. A. Weitz, Science **287**, 627 (2000).

[44] L. Berthier, D. Chandler, and J. P. Garrahan, Europhys. Lett. **69**, 320 (2005).

[45] O. Dauchot, G. Marty, and G. Biroli, Phys. Rev. Lett. **95**, 265701 (2005).

[46] A. Díaz-Sánchez, A. de Candia, and A. Coniglio, J. Phys. A: Math. Gen. **35**, 3359 (2002).

[47] V. Privman and P. Nielaba, Europhys. Lett. **18**, 673 (1992).

[48] J. W. Lee and B. H. Hong, J. Chem. Phys. **119**, 533 (2003).

[49] I. Lončarević, Lj. Budinski-Petković, S. B. Vrhovac, and A. Belić, Phys. Rev. E **80**, 021115 (2009).

[50] I. Lončarević, Lj. Budinski-Petković, and S. B. Vrhovac, Eur. Phys. J. E **24**, 19 (2007).

[51] I. Lončarević, Lj. Budinski-Petković, and S. B. Vrhovac, Phys. Rev. E **76**, 031104 (2007).